

The molecular yo-yo method: Live jump detection improves throughput of single-molecule force spectroscopy for out-of-equilibrium transitions

A. H. Mack,^{1,2, a)} D. J. Schlingman,^{1,3, a)} M. Kamenetska,^{3,4} Robert Collins,³ L. Regan,^{1,3,5} and S. G. J. Mochrie^{1,2,4}

¹⁾*Integrated Graduate Program in Physical and Engineering Biology, Yale University, New Haven CT 06511*

²⁾*Department of Applied Physics, Yale University, New Haven CT 06511*

³⁾*Department of Molecular Biophysics and Biochemistry, Yale University, New Haven CT 06511*

⁴⁾*Department of Physics, Yale University, New Haven CT 06511*

⁵⁾*Department of Chemistry, Yale University, New Haven CT 06511*

(Dated: 15 March 2013)

By monitoring multiple molecular transitions, force-clamp and trap-position-clamp methods have led to precise determinations of the free energies and free energy landscapes for molecular states populated in equilibrium at the same or similar forces. Here, we present a powerful new elaboration of the force-clamp and force-jump methods, applicable to transitions far from equilibrium. Specifically, we have implemented a live jump detection and force-clamp algorithm that intelligently adjusts and maintains the force on a single molecule in response to the measured state of that molecule. We are able to collect hundreds of individual molecular transitions at different forces, many times faster than previously, permitting us to accurately determine force-dependent lifetime distributions and reaction rates. Application of our method to unwinding and rewinding the nucleosome inner turn, using optical tweezers reveals experimental lifetime distributions that comprise a statistically-meaningful number of transitions, and that are accurately single exponential. These measurements significantly reduce the error in the previously measured rates, and demonstrate the existence of a single, dominant free energy barrier at each force studied. A key benefit of the molecular yoyo method for nucleosomes is that it reduces as far as possible the time spent in the tangentially-bound state, which minimizes the loss of nucleosomes by dissociation.

PACS numbers: 68.35.Ja, 61.25.Hq

I. INTRODUCTION

Single-molecule studies of biomolecules and their complexes have led to important new insights into the molecular mechanisms underlying many biological processes. Single-molecule force spectroscopy (SMFS), in particular, has proven a powerful method by which to study the mechanochemistry of molecular motors, including kinesins^{1–3}, myosins^{4–6}, polymerases^{7–11}, helicases^{12–14}, chromatin remodellers^{15–17}, and the ribosome^{18,19}. SMFS has also transformed our understanding of nucleic acid^{20–23} and protein folding^{24–33}, and biological assembly processes, such as chromatin compaction^{34–46}. In all of these cases, the key questions are: What microscopic states are populated at a given force? What are the characteristics of the force-dependent transitions among these states, including what is the distribution of lifetimes for each transition and what is the mean rate of each transition? These quantities determine the relevant free energy landscape of the biomolecules under study, and their diffusion constants for motion within this landscape. In practice, however, the level of detail resolvable in the free energy landscape may be limited by the number of molecular events that can feasibly be observed.

To-date, the most detailed characterizations of biomolecular free energies and free energy landscapes have been

obtained in optical-tweezers-based force-clamp^{28,30,47–49} and trap-position-clamp^{23,31} experiments in which multiple molecular states are in equilibrium with each other at the same or nearly the same force. In such situations, it is often possible to observe hundreds of transitions back and forth among the different molecular states involved. Because of the large number of transitions, the transition rates, and hence the free energies of the states, may be accurately determined^{20–23,29,31–33,40}. By contrast, for molecular states that are not in equilibrium – that is, for molecular states for which spontaneous transitions back and forth are not observable on experimental timescales at a single force – it is more challenging to collect a statistically large-enough data set to be able to determine the transition rates accurately. Most commonly under these circumstances, researchers carry out repeated measurements of the molecular force-versus-extension curve^{24,40,50,51} in order to determine the distribution of transition forces. To increase the rate of data acquisition in force-versus-extension measurements, tandem arrays of independent, identical molecules are often used^{24–27}. Nevertheless, each force-versus-extension curve contains a limited number of transitions, and several practical limitations, such as surface sticking, tether rupture, protein dissociation, *etc.* mean that each molecule is only measurable for a finite period of time. Moreover, a fundamental limitation of the force-versus-extension approach, compared to force-clamp and trap-position-clamp methods, is that the force-dependent lifetime distributions and transition rates are not measured directly. Instead, model-based approaches are required to de-

^{a)}These authors contributed equally to this work.

termine the transition rates from the measured distribution of transition forces, in which it is usually assumed that the transition lifetimes are exponentially distributed at all forces^{52,53}. The force-jump method, in which a force-clamp alternates periodically between a high-force and a low-force⁵⁴⁻⁵⁶, overcomes a number of these difficulties. However, because the force-clamps must be maintained for long enough to ensure that the transitions have taken place, this method is not efficient. In addition, because the force must be maintained at a high value for an extended period of time, the force-jump method is especially vulnerable to tether rupture and other irreversible damage.

The purpose of this paper is to present a powerful new elaboration of the force-clamp and force-jump methods, which we call “the molecular yo-yo method”, that permits the efficient determination of lifetime distributions and transition rates for single molecules, even for molecular states that are not in equilibrium. The key innovation of the molecular yo-yo method to implement a live state-detection and force-clamp algorithm, that intelligently adjusts and maintains the force on a single molecule in real-time, in response to the measured state of the molecule. We describe two simple to implement live jump detection algorithms. The molecular yo-yo method is broadly applicable to out-of-equilibrium molecular transitions of all sorts. Here, to showcase the usefulness of this method, we report its implementation in experiments that seek an improved characterization of the unwinding and rewinding transitions of the nucleosome inner turn, which are out-of-equilibrium at near-physiological salt concentrations³⁴⁻⁴⁶.

The relevant states for nucleosome unwinding and rewinding are illustrated in Fig. 1A³⁶. In this paper, we probe the transition from state 1 to state 0 as shown in Fig. 1B. Although states 1 and 0 are out of equilibrium at any force, nevertheless, using the molecular yo-yo method, we have been able to collect hundreds of molecular transitions, permitting us to accurately determine force-dependent lifetime distributions and force-dependent reaction rates for unwinding and rewinding the nucleosome inner turn. The molecular yo-yo method is especially valuable for studies of nucleosomes because it reduces as far as possible the time spent in the unwound state (state 0), correspondingly reducing the loss of nucleosomes by dissociation in a given period of time. Using this new method, we found that at each force studied, the lifetime distributions are well-described as a single exponential, indicating that the free energy landscapes relevant to winding and unwinding are each dominated by a single free energy barrier. We also demonstrate that the unwinding rates for tethers containing 2, 4 and 8 nucleosomes are accurately 2-, 4-, and 8-fold faster, respectively, than for tethers containing a single nucleosome. This observation implies that nucleosomes on the same tether unwind independently, as has been previously assumed but not proven. Finally, we show that the rates measured using the optical yo-yo method match those determined previously by the more laborious method of making a series of measurements at different forces, using a simple force clamp and force jumping.

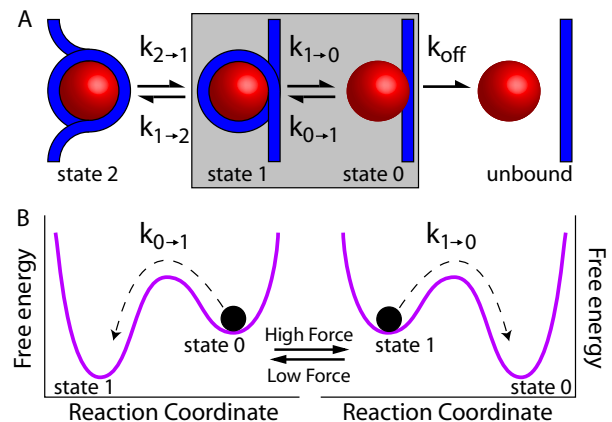


FIG. 1. (A) Schematic of the four microstates for nucleosome unwinding/rewinding³⁶. Histones are red. DNA is blue. For state 2, the nucleosome is fully wrapped by nearly two turns of DNA. For state 1, the outer turn is unwrapped, but the inner turn is wrapped. For state 0, both the outer and inner turns are unwrapped, but the histone octamer remains bound to the DNA. The shaded box encompasses the states and transitions probed in this paper. (B) Schematic illustration of the application of our molecular yo-yo method to the free energy landscape for states not in equilibrium. The rate of transitions from state 1 to state 0 is non-negligible only at high force; the rate of transitions from state 0 to state 1 is non-negligible only at low force. Following every transition, our algorithm detects the molecular state and adjusts the force so that the reverse transition can take place. By toggling between the high and low force configurations we are able to rapidly measure many transitions from a single molecule.

II. MATERIALS AND METHODS

A. DNA preparation and surface attachment

Segments of DNA containing 4200 base-pairs, corresponding to a contour length of 1430 nm, were created from linearized pUC18 plasmids harboring an array of twelve 601 nucleosome positioning sequences (NPSs), a kind gift from Dr. Daniela Rhoades^{57,58}. To facilitate robust attachments between the DNA and a microscope coverslip and between the DNA and the optically-trapped bead, the DNA is labeled with biotin on one end and an amine on the other end. To create DNA-tethered beads, the amine-labeled DNA end is covalently attached to the glass coverslip via a silane PEG N-hydroxysuccinamide linker while the biotin-labeled DNA end binds to a streptavidin coated polystyrene bead⁵⁹.

B. Histone expression and purification

pET vectors containing untagged *Xenopus* H2A, H2B, H3 or H4 were a kind gift from Dr. Karolin Luger. Histones are expressed in *E. coli* BL21-Gold(DE3), extracted from isolated inclusion bodies in buffer containing 7 M GuHCl, and

dialyzed into 8 M urea buffer. Histones are purified first by passage through a Q-sepharose column, and then bound to a Hi-Trap SP column (GE Healthcare Life Sciences), washed with 300 mM NaCl, and eluted with a step gradient to 600 mM NaCl. Finally, the histones are dialyzed into deionized distilled H₂O, lyophilized, and stored at -80°C until needed.

C. Nucleosome reconstitution

Equimolar ratios of the four core histones are combined in buffer containing 7 M GuHCl and dialyzed into buffer containing 2 M NaCl, resulting in octamer formation⁶⁰. After isolation by gel filtration, octamer is mixed with carrier DNA – ultra pure salmon sperm DNA, sheared to 1000 bp (Invitrogen) – and continuously dialyzed into buffer without salt to form nucleosomes. We then assemble nucleosomes *in situ* by flowing a solution of nucleosomes, bound to carrier DNA, at 680 mM NaCl, into our optical tweezers flow cell, which consists of a flow channel cut out of double-sided sticky tape between a microscope coverslip and a microscope slide into which are drilled two holes for fluid inlet and outlet, respectively. *In-situ* nucleosomes exchange between the carrier DNA and the immobilized 601 DNA tether ensures occupancy of the 601 sites. We then flow in a 100 mM NaCl buffer, in preparation for optical tweezers measurements. For experiments discussed here, we prepared arrays of varying numbers of nucleosomes per tether in order to be able to compare rates of unwinding and rewinding with different number of nucleosomes.

D. Optical trapping instrumentation

In the optical trapping setup used for these experiments, the beam from a 1064 nm laser (Ventus IR, Laser Quantum, Stockport, UK) is incident on an acousto-optic deflector (AOD) (IntraAction DTD-274HA6), which serves to optically isolate the laser from the downstream optics, and to control the trapping laser power. Located between the AOD and the microscope objective (Nikon CFI $\times 100$, oil immersion, NA 1.25) is a telescope that expands the beam by a factor of three to ensure that the back pupil of the objective is overfilled, as required for strong trapping. Beyond the objective, the transmitted laser light is incident upon a quadrant photo-diode (QPD) (Phresh Photonics SiQu50-M), located in a plane conjugate to the back focal plane of the microscope condenser lens, where variations in the summed intensity of all four QPD quadrants are linearly proportional to the displacements of a trapped bead from the center of the trap along the beam direction. This method of determining bead position – “back-focal-plane interferometry” (BFPI)⁶¹ – provides a sensitive measure of the force on the bead, which is proportional to the bead displacement from the trap center.

The measurements described in this paper were carried out using an axial pulling geometry in which a piezo-electric translation stage moves the microscope coverslip along the direction of the laser beam, thus applying tension to a surface-

tethered molecule in the axial direction and maintaining a simple geometry at all extensions^{23,62–66}. To make use of the axial pulling geometry, we have implemented a new calibration method that allows conversion from the experimental signals – stage displacement and scattering intensity – to calibrated values of the molecular extension and applied tension. Our calibration procedures are fully described in Ref. 67.

Our axial pulling geometry enables straightforward implementation of a reliable feedback loop that maintains a constant force on the tether⁶⁷. Specifically, the force measured by the QPD is held constant by adjusting the position of a piezo-electric stage (NanoMAX311, Thorlabs). To achieve this force-clamp, we implemented a proportional-integral-derivative (PID) feedback controller using LabView and Labview-MathScript, which carries out the conversion from QPD intensity and piezo-stage position to axial force and tether extension, followed by actuation of the piezo-stage PID control, at a cycle rate greater than 1000 Hz. Data acquisition card PCIe-6343 (National Instruments) is used for both acquisition and output.

When a nucleosome unwinds, the tether length increases by about 25 nm. Concomitantly, the force transiently decreases. However, within 10 ms, our force clamp has adjusted the trap position to increase the tension to the force-clamp value. This response time is limited by the mechanical response of the microscope stage, not by the computation time of our conversion algorithm. In fact, we can flexibly program an arbitrary sequence of forces versus time, jumping out, if necessary, at programmable break points. This flexibility enables the molecular yo-yo method.

In order to sustain meaningful measurements on the same molecular construct for extended periods of time, it is necessary to dynamically correct for any drift in the position of the piezo-stage and in the laser intensity. Since such drift is slow, it is satisfactory to apply a drift correction procedure every ~ 200 s, which we do automatically. Specifically, stage drift is corrected for by measuring the position at which the bead contacts the coverslip, permitting us to update the piezo-stage calibration correspondingly. By holding the bead against the stage and measuring for 100 ms, we are able to establish the bead-coverslip separation to within about 2 nm. To correct for possible laser intensity drift, the force zero is established by placing the bead close to, but not in contact with, the coverslip, so that the tether has a very low extension, and the corresponding force is negligible. This procedure establishes the force to within 0.1 pN.

III. RESULTS AND DISCUSSION

A. Molecular yo-yo method

The molecular yo-yo method operates as follows: At the start time, a high, unwinding force is suddenly applied to the nucleosome in the wound state (state 1). After a period of time at this force, the wound nucleosome transitions to the unwound state (state 0), leading to an increase in extension. By using the preprogrammed force-versus-extension curve of the

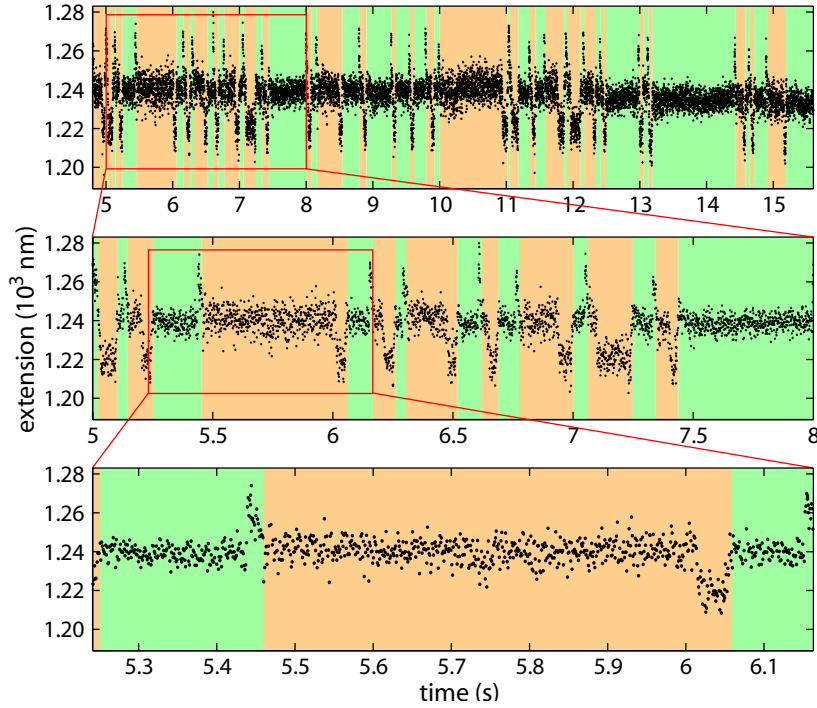


FIG. 2. Unwinding and rewinding the nucleosome inner turn using the optical yo-yo method. (A) Extension versus time while a single nucleosome is repeatedly unwound at an unwinding force of 10.3 pN and rewound at a rewinding force of 3.8 pN over a period of about 11 s. Extension data obtained at the unwinding force is shown with a green background while the extension data obtained at the rewinding force is shown with an orange background. (B) Extension versus time, plotted over a restricted time range, showing four unwinding events from (A). (C) Extension versus time plotted for a further restricted time range, now showing a single molecular yo-yo cycle. The nucleosome unwinds at about 5.44 s and rewinds at about 6.02 s.

states involved, the yo-yo algorithm recognizes the change in state, and, after a short delay, reduces the force to the rewinding force. After a period of time at the rewinding force, the nucleosome transitions back to the wound state (state 1), with a concomitant decrease in extension. The algorithm then recognizes this state change and increases the force to the unwinding force once again. This cycle is then repeated multiple times, and at multiple unwinding and rewinding forces. Importantly in the nucleosome context, the molecular yo-yo algorithm reduces as far as possible histone-DNA dissociation from the unwound state by minimizing the time the nucleosome spends in the unwound state. Each measured dwell time at a given force contributes to the lifetime distribution at that force.

Fig. 2A shows a representative extension versus time trace that covers twenty-eight repeats of the molecular yo-yo live jump detection algorithm that detects and triggers on both unwinding and rewinding events. Fig. 2B highlights nine of these cycles, and Fig. 2C a single cycle. In Fig. 2C, for times prior to 5.25 s, the nucleosome inner turn is wound and the force is 3.8 pN. At 5.25 s, the current yo-yo cycle is initiated, when the force-clamp steps up to 10.3 pN, as indicated by the green background. This force jump is signaled by a corresponding stepwise increase in the extension trace of Fig. 2C, as the DNA tether stretches further in response to the increased force. The nucleosome remains wound at

10.3 pN for approximately 0.2 s until it unwinds at 5.44 s, signaled by a jump in the extension of about 25 nm. Thus, during this particular cycle, the lifetime of the wound state at 10.3 pN was measured to be 0.2 s. The nucleosome remains unwound at 10.3 pN for approximately 5 ms, which is the period of time required for the yo-yo algorithm to recognize the unwinding event. Once the transition to the unwound state has been recognized, the force-clamp steps down to 3.8 pN, as indicated by the orange background. The extension decreases concomitantly, because the DNA tether stretches less at the reduced force. The nucleosome remains unwound at 3.8 pN until 6.01 s before rewinding. This gives us a measurement of the lifetime of the unwound state at 3.8 pN to be 0.55 s. At 6.02 s, rewinding is signaled by a decrease in the extension of about 22 nm. Once the rewinding transition is recognized, the next yo-yo cycle is then initiated by returning the force to 10.3 pN. Triggering on both rewinding and unwinding events, as in Fig. 2, minimizes unnecessary measurements after the transition has occurred, and leads to a significantly faster data acquisition rate than otherwise would be possible.

B. Live jump detection algorithm

We have implemented two jump detection algorithms, one for unwinding and one for rewinding. Both jump detection

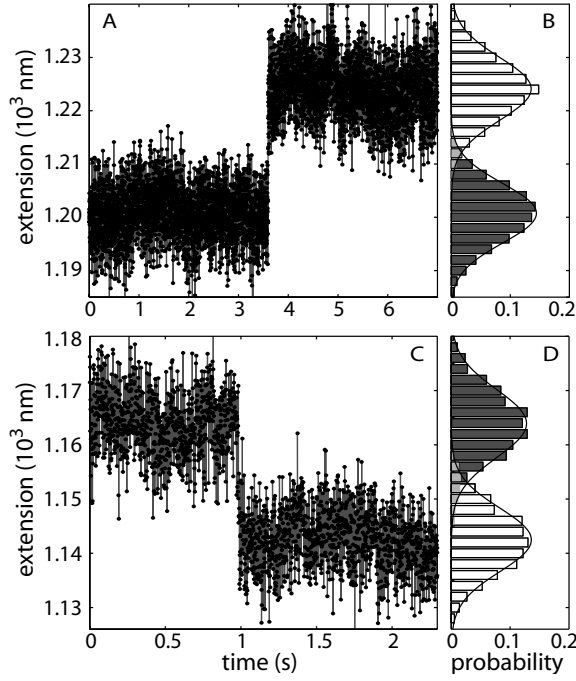


FIG. 3. Extension versus time of individual nucleosomes held at fixed force and their corresponding extension distributions. (A) Extension versus time of a single nucleosome, held at a fixed unwinding force of 10.3 pN, measured every 1 ms and plotted as connected dots. At 3.6 s after the unwinding force is applied, an unwinding event is evident, in which the extension jumps by 25 nm. (B) Experimental probability distributions for the extension before (gray bars) and after (white bars) the unwinding event. These histograms correspond to 3500 (gray) and 3300 (white) measurements of the extension with a bin size of 2 nm. The smooth curves are Gaussians, each plotted using the mean and standard deviation of the respective experimental distributions: $\sigma_1 = 5.9$ nm and $\sigma_0 = 5.6$ nm, for state 1 and state 0, respectively, at this force. (C) Extension versus time of a single nucleosome, held at a fixed rewinding force of 3.8 pN, measured every 1 ms and plotted as connected dots. At 0.98 s after the force is applied, a rewinding event is observed as a stepwise 22 nm decrease in the extension. (D) Probability distributions determined before (gray bars) and after (white bars) the rewinding event with bins of size 2 nm. These histograms correspond to 986 (gray) and 1314 (white) measurements of the extension. The smooth curves are Gaussians, each plotted using the mean and standard deviation of the respective experimental distributions: $\sigma_0 = 5.9$ nm and $\sigma_0 = 6.2$ nm, for state 1 and state 0, respectively, at this force.

algorithms rely on comparing live extension to preceding extension measurements. Fig. 3A shows an example extension of a tether during a nucleosome unwinding event with no detection. At time zero, a force-clamp of 10.3 pN is applied to a single nucleosome. For a period of approximately 3.6 s, the nucleosome in state 1 remains stable at this force, while the extension fluctuates about a mean of about 1200 nm. At 3.6 s, the nucleosome unwinds into state 0, signaled by an increase in extension caused by about 25 nm of DNA being released. Subsequently, state 0 is stable, with its extension fluctuating about a mean of 1225 nm. In Fig. 3B, histograms

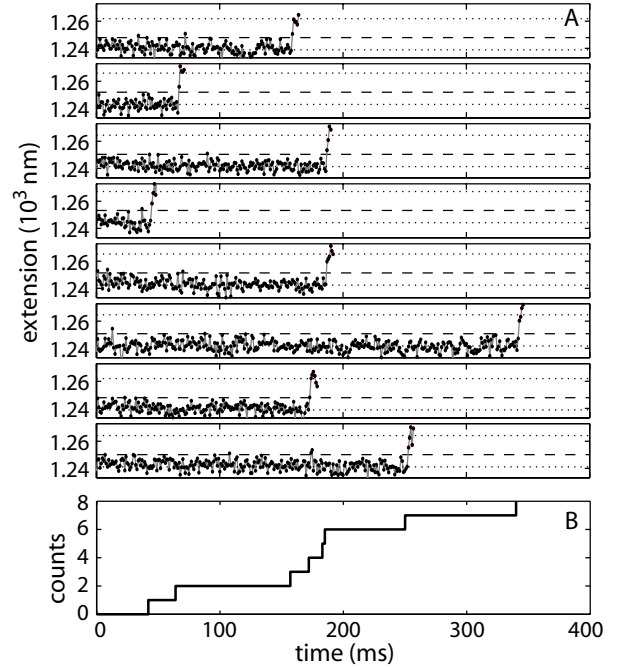


FIG. 4. Examples of individual nucleosome unwinding event detection. (A) Eight extension versus time traces at an unwinding force of 10.3 pN, each showing an example unwinding event recognized by our jump detection method. In each panel, the black dots connected by gray lines represent the extension measurement. The lower dotted line corresponds to the mean of the n_1 (40) points measured before the jump, and represents the extension of state 1, the wound state. The upper dotted line represents the extension of state 0, the unwound state, taken as the wound states extension plus 25 nm. The dashed line is 10 nm from the lower dotted line (state 1), and represents the threshold extension for jump detection in each trace. (B) Count of the number of unwinding events versus time, determined from the eight example traces shown in (A).

of the measured extension, represented as probabilities, before (gray) and after (white) the unwinding transition agree well with overlaid Gaussian distributions, plotted using the mean and standard deviations of the respective measured extension distributions.

Similarly, Fig. 3C shows an example nucleosome rewinding event with no detection. At time zero, a force-clamp of 3.8 pN is applied to a single nucleosome, initially in state 0 (unwound). For a period of approximately 0.98 s, the nucleosome in state 0 remains stable at this force, while the extension fluctuates about a mean of about 1163 nm. At approximately 0.98 s, the nucleosome rewinds into state 1, signaled by a decrease in extension of about 22 nm. Subsequently, state 1 is stable, with its extension fluctuating about a mean of 1141 nm. In Fig. 3D, histograms of the measured extension, represented as probabilities, before (gray) and after (white) the unwinding transition agree well with overlaid Gaussian distributions, plotted using the mean and standard deviations of the respective measured extension distributions. These data were collected at a rate of 1 kHz, where extension fluctuations effec-

tively correspond to uncorrelated, white noise.

To determine in real-time whether an unwinding transition has occurred, our yo-yo algorithm looks back at the previous $n_1 + n_2$ extension measurements. If all of the immediately preceding n_1 measurements exceed the mean of the n_2 measurements previous to those n_1 measurements by more than a threshold value (Δ_1), then the yo-yo algorithm recognizes that a jump in extension has occurred. To assess this simple scheme for false positives, we inquire: What is the probability that the algorithm recognizes a transition from state 1 to state 0, when in fact none occurred? The probability that a single point exceeds the threshold, when the nucleosome remains in state 1, may readily be seen to be equal to

$$P = \frac{1}{2} \operatorname{erfc} \left(\frac{\Delta_1}{\sqrt{2(1 + \frac{1}{n_2})} \sigma_1} \right) \simeq \frac{1}{2} \operatorname{erfc} \left(\frac{\Delta_1}{\sqrt{2} \sigma_1} \right), \quad (1)$$

where erfc is the complementary error function, σ_1 is the standard deviation of the extension fluctuations in state 1, and Δ_1 is the difference in extension between the threshold extension and the mean extension of state 1. The factor $(1 + 1/n_2)$ accounts for the expected variance in the mean extension determined from n_2 measurements. All of the unwinding yo-yo measurements presented in this paper employed $n_1 = 5$ and $n_2 = 40$. With $\sigma_1 = 5.9$ nm, as found experimentally at 10.3 pN, it follows that $P = 0.031$. Given the specified conditions for recognizing the transition, the probability of a false positive is P^{n_1} , leading to a false negative probability of $(0.031)^5 = 2.9 \times 10^{-8}$, which we consider entirely acceptable. Similar considerations apply to unwinding at other forces.

Fig. 4A shows eight example nucleosome unwinding events, as detected by our jump detection algorithm. In each case, the measurement begins with the nucleosome in the state 1 (wound) and with the application of the unwinding force of 10.3 pN at time zero. After a variable time interval, the nucleosome unwinds into state 0. In each case, after about 5 ms, corresponding to $n_1 = 5$, the jump detection algorithm registers the unwinding transition and reduces the force, having measured the lifetime of state 1 at the unwinding force. In all cases, the transition is abrupt and is promptly detected by the algorithm. In each panel, the lower dotted line corresponds to the mean of the previous $n_2 = 40$ points before the jump, and represents the extension corresponding to state 1. The upper dotted line corresponds to the mean extension of the unwound state at an extension 25 nm higher than the lower dotted line. The dashed line represents the threshold, described previously, and is located $\Delta_1 = 11$ nm above the mean extension of state 1. Fig. 4B summarizes the cumulative number of unwinding events versus time, determined from the measurements of Fig. 4A.

We use a modified jump detection algorithm for nucleosome rewinding. At the beginning of this protocol, the extension of a nucleosome in state 1 is determined by a 1 s extension measurement at the rewinding force. The extension of state 0 at the rewinding force is then taken to be the extension of state 1 plus 23 nm. Once the force is jumped to the rewinding force, our algorithm registers a rewinding event when the mean of the previous n_1 extension measurements lies within a

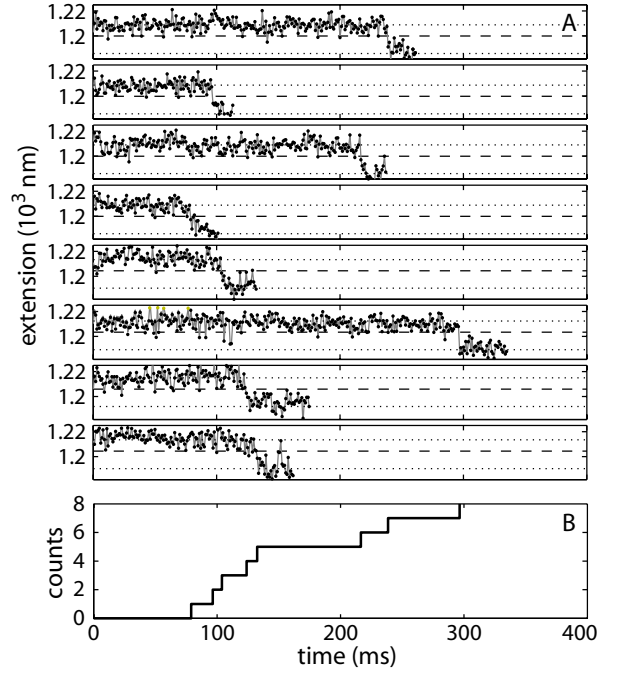


FIG. 5. Examples of individual nucleosome rewinding event detection. (A) Eight extension versus time traces at a rewinding force of 3.8 pN, each showing an example rewinding event recognized by our rewinding jump detection method. In each panel, the black dots connected by gray lines represent the extension measurement. The lower dotted line corresponds to the previously-determined extension of state 1 at 3.8 pN. The upper dotted line represents the extension of state 0, taken as the extension of state 1 plus 23 nm. The dashed line, 10 nm from the lower dotted line (state 1), represents the threshold extension for jump detection in these data. (B) Count of the number of rewinding events versus time, determined from the eight example traces shown in (A).

threshold value, Δ_1 , of the extension of state 1. In this case, the probability of falsely identifying a transition, when none has occurred, is

$$P = \frac{1}{2} \operatorname{erfc} \left(\frac{\Delta_1 \sqrt{n_1}}{\sqrt{2} \sigma_1} \right). \quad (2)$$

Fig. 5A shows eight example nucleosome rewinding events, as detected by this algorithm. In each case, the measurement begins with the nucleosome in the state 0 and with the application of the rewinding force of 3.8 pN at time zero. After a variable time interval, the nucleosome rewinds into state 1. Then, after a time that can be seen to vary from 10 to 40 ms, the jump detection algorithm registers the rewinding transition and increases the force, having measured the lifetime of state 0 at the rewinding force. In all cases, the transition is unambiguous and is readily detected by the algorithm, although not as rapidly as in the case of unwinding. For these example rewinding events, for which $\sigma = 6$ nm, $n_1 = 40$, and $\Delta_1 = 10$ nm, a false-positive jump detection occurs with a probability of 3×10^{-29} , effectively impossible on experimental time-scales. Fig. 5B summarizes the cumulative number of

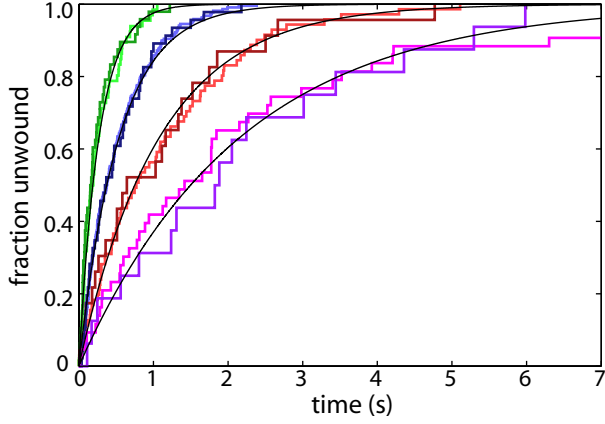


FIG. 6. Cumulative fraction of nucleosomes unwound versus time at 10.3 pN determined on tethers with 8 (green), 4 (blue), 2 (red), or 1 (purple) nucleosomes. Each curve corresponds to measurements performed on a single tether. Each step in the staircases corresponds to an independent unwinding event. The smooth curves are exponentials with rates $8k$, $4k$, $2k$, and k , where k is determined by the maximum likelihood method from the single nucleosome data⁴⁵. The apparent rate scales with the number of nucleosomes. Measurements on different tethers give the same rate for single nucleosome unwinding.

rewinding versus time, determined from the measurements of Fig. 5A.

C. Distribution of lifetimes at fixed force

To determine the lifetime distribution of state 1 or state 0 at each force studied, we count the cumulative number of unwinding or rewinding events as a function of time, as indicated in Fig. 4B and Fig. 5B. Normalizing by the total number of counts, these collections of unwinding and rewinding times determine the cumulative fraction of nucleosome inner turns unwound and wound, respectively, as a function of time, at a given force. In Fig. 6, we show unwinding data at 10.3 pN obtained on tethers with one, two, four and eight nucleosomes in purple, red, blue and green respectively. We plot two curves each for 1, 2, 4, and 8 nucleosomes. Each was obtained in separate experiments with different tethers and nucleosomes, demonstrating individual tether-to-tether and nucleosome-to-nucleosome repeatability.

If we assume first-order unwinding (rewinding) kinetics, the probability that a nucleosome initially in state 1 (or 0) will have undergone unwinding to state 0 (or 1) within a time t after initiation of the force clamp is given by an exponential function:

$$p = 1 - e^{-kt}, \quad (3)$$

where k is the unwinding (rewinding) rate. For independent nucleosomes, we expect the apparent unwinding rate for 2, 4, and 8 nucleosomes to be 2 times, 4 times and 8 times, respectively, the rate for a single nucleosome. The smooth curves

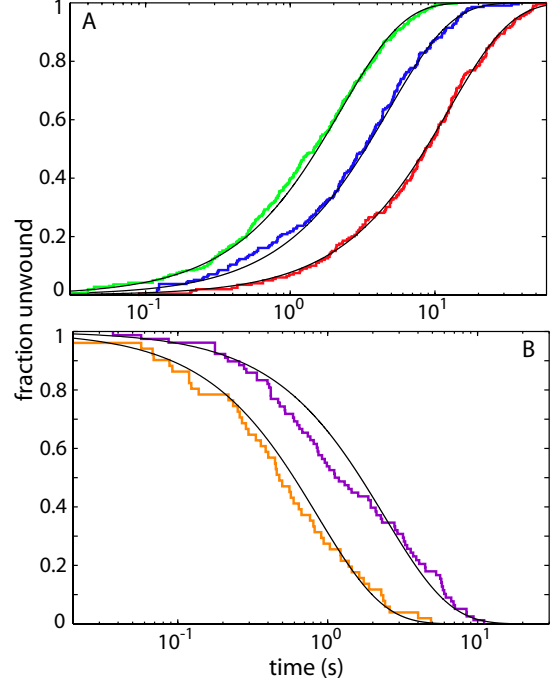


FIG. 7. Cumulative fraction of nucleosomes unwound versus time for unwinding and rewinding determined using the molecular yo-yo method. (A) Distribution of unwinding times at 8.5 pN (red), 9.4 pN (green), and 10.3 pN (blue) shown using a logarithmic time axis, with distributions determined using 201, 211, and 354 unwinding events, respectively. Each step is an independent unwinding event. (B) Distributions of rewinding times at 3.3 pN (orange) and 3.8 pN (purple), after unwinding at 14.1 pN, determined using 66 and 78 rewinding events, respectively. In both (A) and (B), the corresponding, overlaid smooth black curves are exponentials with rates determined by the maximum likelihood method.

in Fig. 6 correspond to exponentials with rate set according to this rule, using the maximum likelihood value of the unwinding rate determined from data obtained on a single nucleosome. Evidently, the model curves provide an excellent description of the behavior with 1, 2, 4, and 8 nucleosomes. This observation directly demonstrates that at the forces studied nucleosomes on the same DNA tether unwind independently, as has previously been assumed but not proven.

Fig. 7A displays the distributions of unwinding times, using a logarithmic time axis, at 8.5, 9.4, and 10.3 pN, each determined from multiple nucleosomes, collected together to yield a single distribution at each force. Similarly, Fig. 7B displays the distribution of rewinding times at 3.3 and 3.8 pN for nucleosomes, that were unwound at 14.1 pN. For both Fig. 7A and B, each distribution is represented as the fraction of nucleosomes unwound. The collected events at each force constitute a sufficiently large data set (201, 211, 354, 66 and 78 transitions at 8.5, 9.4, 10.3, 3.3 and 3.8 pN, respectively) to enable us to not only determine the unwinding rate at the force in question but also to test whether an exponential distribution of lifetimes is a correct description. The solid black lines in Fig. 7A and B correspond to EQ. 3 calcu-

lated using the maximum likelihood values of the unwinding and rewinding rates respectively. Evidently, this model provides an excellent description of our measured lifetime distributions with zero adjustable parameters, indicating that a single exponential lifetime distribution is the correct description, and that the transition rates are 0.062 ± 0.004 , 0.16 ± 0.01 , 0.40 ± 0.02 , 1.2 ± 0.1 , and $0.38 \pm 0.04 \text{ s}^{-1}$ at 8.5, 9.4, 10.3, 3.3, and 3.8 pN, respectively. To objectively assess how well EQ. 3 accounts for the measured lifetime distributions, we have binned the unwinding lifetime measurements shown in Fig. 7 into logarithmically-sized bins⁶⁸. Binning the data to obtain the distribution of lifetimes ensures that the number of counts in the different bins are statistically independent of one another, which is not the case for the cumulative distributions of Figs. 6 and 7. It also permits us to simply determine the standard error for each bin as the square-root of the number of counts in each bin. The corresponding histograms, including error bars, are compared with the model distribution corresponding to EQ. 3 in Fig. 8. To determine the goodness of fit, we calculated the reduced chi-squared:

$$\chi^2 = \frac{1}{n-1} \sum_{i=1}^n \frac{(O_i - E_i)^2}{E_i^2}, \quad (4)$$

where the sum runs from 1 to $n = 13$ bins, O_i is the observed number of counts in bin i , and E_i is the expected number of counts in bin i ⁶⁹. The reduced χ^2 -values are 0.58, 1.3, and 1.21, for the unwinding distributions at 8.5, 9.4, and 10.3 pN, respectively. For the rewinding distribution at 3.3 and 3.8 pN, the reduced χ^2 -values are 1.0 and 1.3, respectively. Thus, in every case, χ^2 is close to unity, indicating that there is not a statistically significant deviation between the data and the model of EQ. 3 at any of the forces studied.

D. Force dependent unwinding and rewinding rates of the nucleosome inner turn

Fig. 9 summarizes our measurements of the force-dependent rates of unwinding and rewinding the nucleosome inner turn, obtained with the molecular yo-yo method. For comparison, Fig. 9 also includes our previously published results for these rates⁴⁵. Evidently, measurements of the nucleosome inner turn unwinding and rewinding rates, obtained using the molecular yo-yo method, show good agreement with those obtained previously. At a given force, however, the number of transitions available via the yo-yo method is several-fold larger than the number previously available, yielding values for the transition rates that are accurate to within about 10%. Thus, in future nucleosome studies the molecular yo-yo method will enable us to resolve subtle differences in the kinetics of different nucleosomes, with different histone variants and modifications, for example.

E. Conclusion

In this paper, we have introduced and demonstrated a powerful elaboration of the force clamp method, called the molec-

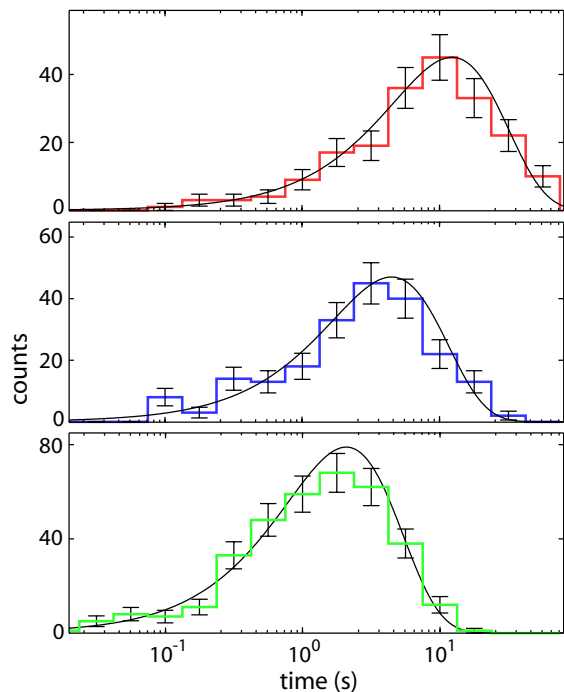


FIG. 8. Histogram of nucleosome unwinding times shown using a logarithmic time axis. Unwinding times at 8.5 pN (red), 9.4 pN (blue), and 10.3 pN (green) were logarithmically-binned with distributions determined using 201, 211, and 354 unwinding events, respectively. Each bin is a factor of 3 longer than the preceding bin. The histogram of the number of events with lifetimes in each time bin is displayed as a staircase. The standard error for the number of counts in each bin, shown as the error bar, is determined by counting (Poisson) statistics. An exponential distribution, corresponding to the characteristic unwinding rate, determined by the maximum likelihood method, is overlaid as the thin continuous line.

ular yo-yo, that is broadly applicable to molecular transitions that are far from equilibrium. The molecular yo-yo method implements a live jump-detection and force-clamp algorithm, that intelligently adjusts and maintains the force on a single molecule, in response to the measured state of that molecule. Thus, we are able to realize hundreds of individual molecular transitions between molecular states at different forces, permitting us to accurately determine force-dependent lifetime distributions and reaction rates. Compared to force-versus-extension measurements, the molecular yo-yo method directly measures these key quantities, while maximizing data acquisition rate and efficiency. Compared to force-jump measurements, the molecular yo-yo method minimizes the time spent at high force, where molecular complexes can dissociate. We presented measurements detailing the specific application of the molecular yo-yo to unwinding and rewinding the nucleosome inner turn, using optical tweezers. Because the molecular yo-yo minimizes the time spent in the unwound state (state 0), nucleosome dissociation is also minimized, permitting hundreds of transitions to be obtained from a single construct before nucleosome dissociation ends the measurement.

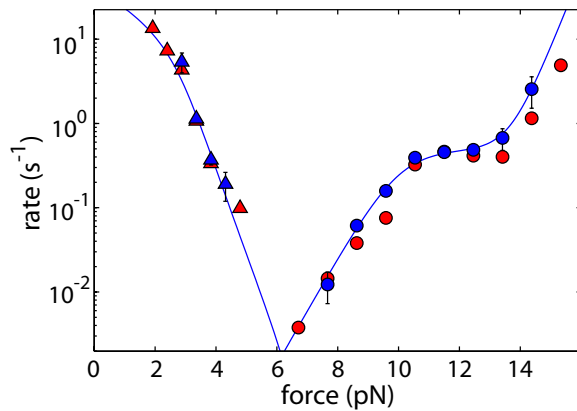


FIG. 9. Unwinding and rewinding rates of the nucleosome inner turn plotted as a function of force. Shown as blue circles are the unwinding rates obtained from 12 nucleosomes undergoing a total of 1086 unwinding events with the molecular yo-yo method. Shown as blue triangles are the rewinding rates, obtained using the molecular yo-yo method, from 6 nucleosomes undergoing a total of 167 rewinding events. The previously published unwinding and rewinding rates are shown as red circles and triangles, respectively. These data were acquired using a total of 334 nucleosomes with 265 unwinding events and 136 rewinding events.

Our molecular yo-yo measurements of unwinding and rewinding the nucleosome inner turn reveal experimental lifetime distributions that are accurately single exponential, indicating the existence of a single dominant free energy barrier between states 1 and 0. We also demonstrate that the unwinding rates for tethers containing 2, 4, and 8 nucleosomes are accurately 2-, 4-, and 8-fold faster, respectively, than for tethers containing a single nucleosome. This observation implies that nucleosomes on the same tether unwind independently, as has been previously assumed but not proven. Finally, we note that improved throughput is not the only benefit allotted by live jump detection, only the most obvious. A variety of more elaborate experimental force protocols enabling new measurements are clearly made possible with variations of the technique presented here. Additionally, live jump detection methods are transferable to other SMFS methods, such as those that employ an atomic force microscope.

ACKNOWLEDGMENTS

We thank J. Antonypillai, E. Dufresne, R. Illagan, P. Koo, L.-A. Metskas, F. Sigworth, Y. Zhao, N. Sawyer, E. Speltz, A. Schloss, J. Chen, and A. Zhou for valuable discussions. This work was supported by the Raymond and Beverly Sackler Institute for Biological, Physical and Engineering Sciences and NSF PoLS 1019147. D.J.S. acknowledges the support of a NSF Graduate Research Fellowship. M. K. acknowledges the support of NSF Postdoctoral Research Fellowship in Biology Award DBI 1103715.

- ¹S. M. Block, L. S. B. Goldstein, and B. J. Schnapp, *Nature* **348** (1990).
- ²K. Svoboda, C. Schmidt, B. Schnapp, S. Block, et al., *Nature* **365**, 721 (1993).
- ³S. C. Kuo and M. P. Sheetz, *Science* **260**, 232 (1993).
- ⁴J. E. Molloy, J. E. Burns, J. Kendrick-Jones, R. T. Tregear, and D. C. S. White, *Nature* **378**, 209 (1995).
- ⁵J. S. Wolenski, R. E. Cheney, M. S. Mooseker, and P. Forscher, *J. Cell Sci.* **108**, 1489 (1995).
- ⁶C. Veigel, L. M. Coluccio, J. D. Jontes, J. C. Sparrow, R. A. Milligan, and J. E. Molloy, *Nature* **398**, 530 (1999).
- ⁷M. D. Wang, M. J. Schnitzer, H. Y. R. Landick, J. Gelles, and S. M. Block, *Science* **282**, 902 (1998).
- ⁸N. R. Forde, D. Izhaky, C. R. Woodcock, G. J. Wuite, and C. Bustamante, *Proc. Natl. Acad. Sci. USA* **99**, 11682 (2002).
- ⁹E. A. Abbondanzieri, W. J. Greenleaf, J. W. Shaevitz, R. Landick, and S. M. Block, *Nature* **438**, 460 (2005).
- ¹⁰K. M. Herbert, A. L. Porta, B. J. Wong, R. A. Mooney, K. C. Neuman, R. Landick, and S. M. Block, *Cell* **125**, 1083 (2006).
- ¹¹L. Bintu, M. Kopaczynska, C. Hodges, L. Lubkowska, M. Kashlev, and C. Bustamante, *Nature Structural and Molecular Biology* **18**, 1394 (2011).
- ¹²T. T. Perkins, H. W. Li, R. V. Dalal, J. Gelles, and S. M. Block, *Biophys. J.* **86**, 1640 (2004).
- ¹³S. Dumont, W. Cheng, V. Serebrov, R. K. Beran, I. Tinoco, A. Pyle, and C. Bustamante, *Nature* **439**, 105 (2006).
- ¹⁴D. S. Johnson, L. Bai, B. Y. Smith, S. S. Patel, and M. D. Wang, *Cell* **129**, 1299 (2007).
- ¹⁵G. Lia, E. Praly, H. Ferreira, C. Stockdale, Y. C. Tse-Dinh, D. Dunlap, V. Croquette, D. Bensimon, and T. Owen-Hughes, *Molecular Cell* **21**, 417 (2006).
- ¹⁶Y. Zhang, C. L. Smith, A. Saha, S. W. Grill, S. Mihardja, S. B. Smith, B. R. Cairns, C. L. P. CL, and C. Bustamante, *Molecular Cell* **24**, 559 (2006).
- ¹⁷G. Sirinakis, C. R. Clapier, Y. Gao, R. Viswanathan, B. R. Cairns, and Y. Zhang, *EMBO J.* **30**, 2364 (2011).
- ¹⁸J.-D. Wen, L. Lancaster, C. Hodges, A.-C. Zeri, S. H. Yoshimura, H. F. Noller, C. Bustamante, and I. Tinoco, *Nature* **452**, 598 (2008).
- ¹⁹X. Qu, J.-D. Wen, L. Lancaster, H. F. Noller, C. Bustamante, and I. Tinoco, *Nature* **475**, 118 (2011).
- ²⁰J. Liphardt, B. Onoa, S. B. Smith, I. Tinoco, and C. Bustamante, *Science* **292**, 733 (2001).
- ²¹M. T. Woodside, P. C. Anthony, W. M. Behnke-Parks, L. Larizadeh, D. Herschlag, and S. Block, *Science* **314**, 1001 (2006).
- ²²W. J. Greenleaf, K. L. Frieda, D. A. N. Foster, M. T. Woodside, and S. M. Block, *Science* **319**, 630 (2008).
- ²³M. de Messieres, B. Brawn-Cinani, and A. L. Porta, *Biophys. J.* **100**, 2736 (2011).
- ²⁴M. Rief, M. G. F. Oesterhelt, J. M. Fernandez, and H. E. Gaub, *Science* **276**, 1109 (1997).
- ²⁵P. E. Marszalek, H. Lu, H. Li, M. Carrion-Vazquez, A. F. Oberhauser, K. Schulten, and J. M. Fernandez, *Nature* **402**, 100 (1999).
- ²⁶H. Li, A. F. Oberhauser, S. D. Redick, M. Carrion-Vazquez, H. P. Erickson, and J. M. Fernandez, *Proc. Nat. Acad. Sci. USA* **98**, 10682 (2001).
- ²⁷R. B. Best, S. B. Fowler, J. L. Toca-Herrera, and J. Clarke, *Proc. Nat. Acad. Sci. USA* **99**, 12143 (2002).
- ²⁸J. M. Fernandez and H. Li, *Science* **303**, 1674 (2004).
- ²⁹C. Cecconi, E. A. Shank, C. Bustamante, and S. Marqusee, *Science* **309**, 2057 (2005).
- ³⁰J. Brujic, R. I. Hermans, K. A. Walther, and J. M. Fernandez, *Nature Physics* **2**, 282 (2006).
- ³¹J. C. M. Gebhardt, T. Bornschlogl, and M. Rief, *Proc. Nat. Acad. Sci. USA* **107**, 2013 (2010).
- ³²Y. Gao, G. Sirinakis, and Y. Zhang, *J. Am. Chem. Soc.* **133**, 12749 (2011).
- ³³H. Yua, X. Liu, K. Neupane, A. N. Gupta, A. M. Brigley, A. Solanki, I. Sosova, and M. T. Woodside, *Proc. Nat. Acad. Sci. USA* **109**, 5283 (2012).
- ³⁴Y. Cui and C. Bustamante, *Proc. Nat. Acad. Sci. USA* **97**, 127 (2000).
- ³⁵M. L. Bennink, S. H. Leuba, G. H. Leno, J. Zlatanova, B. G. de Grooth, and J. Greve, *Nature Structural Biology* **8**, 606 (2001).
- ³⁶B. Brower-Toland, C. L. Smith, R. C. Yeh, J. T. Lis, C. L. Peterson, and M. D. Wang, *Proc. Nat. Acad. Sci. USA* **99**, 1960 (2002).

- ³⁷B. Brower-Toland, D. A. Wacker, R. M. Fulbright, J. T. Lis, W. L. Kraus, and M. D. Wang, *J. Mol. Bio.* **346**, 135 (2005).
- ³⁸G. J. Gemmen, R. Sim, K. A. Haushalter, P. C. Ha, J. T. Kadonaga, and D. E. Smith, *J. Mol. Bio.* **351**, 89 (2005).
- ³⁹L. H. Pope, M. L. Bennink, K. A. van Leijenhorst-Groener, D. Nikova, J. Greve, and J. F. Marko, *Biophysical Journal* **88**, 3572 (2005).
- ⁴⁰S. Mihardja, A. J. Spakowitz, Y. Zhang, and C. Bustamante, *Proc. Nat. Acad. Sci. USA* **103**, 15871 (2006).
- ⁴¹M. Kruithof and J. van Noort, *Biophys. J.* **96**, 3708 (2009).
- ⁴²M. Kruithof, F.-T. Chien, A. Routh, C. Logie, D. Rhodes, and J. van Noort, *Nature Structural and Molecular Biology* **16**, 534 (2009).
- ⁴³M. A. Hall, A. Shundrovsky, L. Bai, R. M. Fulbright, J. T. Lis, and M. D. Wang, *Nature Structural and Molecular Biology* **16**, 124 (2009).
- ⁴⁴M. Simon, J. A. North, J. C. Shimko, R. A. Forties, M. B. Ferdinand, M. Manohar, M. Zhang, R. Fishel, J. J. Ottesen, and M. G. Poirier, *Proc. Nat. Acad. Sci. USA* **108**, 12711 (2011).
- ⁴⁵A. H. Mack, D. J. Schlingman, R. Ilagan, L. Regan, and S. G. J. Mochrie, *Journal of Molecular Biology* **423**, 687 (2012).
- ⁴⁶L. Mollazadeh-Beidokhti, F. Mohammad-Rafiee, and H. Schiessel, *Biophysical Journal* **102**, 2235 (2012).
- ⁴⁷R. M. Simmons, J. T. Finer, S. Chu, and J. A. Spudich, *Biophysical Journal* **70**, 1813 (1996).
- ⁴⁸K. Visscher and S. M. Block, *Methods Enzymol.* **298**, 460 (1998).
- ⁴⁹A. F. Oberhauser, P. K. Hansma, M. Carrion-Vazquez, and J. M. Fernandez, *Proc. Nat. Acad. Sci.* **98**, 468 (2001).
- ⁵⁰J. Gebhardt, T. Bornschlöggl, and M. Rief, *Proceedings of the National Academy of Sciences* **107**, 2013 (2010).
- ⁵¹T. Strunz, K. Oroszlan, R. Schäfer, and H. Güntherodt, *Proceedings of the National Academy of Sciences* **96**, 11277 (1999).
- ⁵²O. Dudko, J. Mathé, A. Szabo, A. Meller, and G. Hummer, *Biophysical Journal* **92**, 4188 (2007).
- ⁵³O. K. Dudko, G. Hummer, and A. Szabo, *Phys. Rev. Lett.* **96**, 108101 (2006).
- ⁵⁴P. T. X. Li, D. Collin, S. B. Smith, C. Bustamante, and I. Tinoco, *Biophysical Journal* **90**, 250 (2006).
- ⁵⁵C. M. Kaiser, D. H. Goldman, J. D. Chodera, I. Tinoco Jr., and C. Bustamante, *Science* **334**, 1723 (2011).
- ⁵⁶P. J. Elms, J. D. Chodera, C. Bustamante, and S. Marqusee, *Proc. Nat. Acad. Sci. USA* **109**, 3796 (2012).
- ⁵⁷P. T. Lowary and J. Widom, *J. Mol. Bio.* **276**, 19 (1998).
- ⁵⁸V. A. Huynh, P. J. Robinson, and D. Rhodes, *J. Mol. Bio.* **345**, 957 (2005).
- ⁵⁹D. J. Schlingman, A. H. Mack, S. G. J. Mochrie, and L. Regan, *Colloids and Interfaces B: Biointerfaces* **83**, 91 (2011).
- ⁶⁰K. Luger, T. J. Rechsteiner, and T. J. Richmond, *Methods Mol Biol.* **119**, 1 (1999).
- ⁶¹F. Gittes and C. F. Schmidt, *Optics Letters* **23**, 7 (1998).
- ⁶²A. Clapp, A. Ruta, and R. Dickinson, *Review of Scientific Instruments* **70**, 2627 (1999).
- ⁶³K. Neuman, E. Abbondanzieri, and S. Block, *Optics letters* **30**, 1318 (2005).
- ⁶⁴C. Deufel and M. D. Wang, *Biophys. J.* **90**, 657 (2006).
- ⁶⁵Y.-F. Chen, G. A. Blab, and J.-C. Meiners, *Biophys. J.* **96**, 4701 (2009).
- ⁶⁶N. Forns, S. de Lorenzo, M. Manos, K. Hayashi, J. Huguet, and F. Ritort, *Biophysical Journal* **100**, 1765 (2011).
- ⁶⁷A. H. Mack, D. J. Schlingman, L. Regan, and S. G. J. Mochrie, *Rev. Sci. Instr.* **83**, 103106 (2012).
- ⁶⁸F. J. Sigworth and S. M. Sine, *Biophysical Journal* **52**, 1047 (1987).
- ⁶⁹J. Taylor, *An introduction to error analysis: the study of uncertainties in physical measurements* (Univ Science Books, 1997).